Microwave Circuit Design by Means of Direct Decomposition in the Finite-Element Method

Valentín de la Rubia and Juan Zapata, *Member, IEEE*

***Abstract*—In this paper, a domain decomposition approach for design purposes is proposed. The analysis domain is divided into subdomains according to the arbitrarily shaped parts that should be modified in the synthesis process. A full-wave matrix-valued transfer function describes each decomposition subdomain, namely, an admittance-type matrix. Field continuity between subdomains is directly enforced by an admittance matrix connection. This methodology makes it possible to analyze only those parts of the analysis domain that are supposed to evolve in order to satisfy the design specifications. Furthermore, several modifications in the shape of the components are allowed as a consequence of the easy matrix connection process, where the consideration of different admittance-type matrices or absence of them gives rise to distinct geometric structures. A model order reduction technique is also considered for fast frequency sweeping. Finally, several numerical examples illustrate the capabilities of the proposed procedure, as well as its accuracy.**

***Index Terms*—Admittance matrix, design automation, design methodology, domain decomposition methods (DDMs), finite-element methods (FEMs), piecewise (PCW) linear approximation, reduced-order systems.**

I. Introduction

MICROWAVE designs are currently complex enough for requiring full-wave design techniques, demanding computer-aided design (CAD). Most numerical methods are conceived as analysis tools, but current interests encourage us to go beyond simple analysis because a wide range of analyses ought to be carried out when developing a design by means of optimization processes.

The finite-element method (FEM) is widely known for its flexibility and reliability, but is still merely thought of as an analysis tool due to its rather time-consuming characteristics, especially when dense meshing and high-frequency resolution over a wide band are demanded. Although a 2-D FEM analysis substantially reduces its computational costs and makes it compatible with CAD [1], there is still intensive research to be carried out in the 3-D case. Over the last three decades, a considerable effort has been made in speeding up the solution time for the FEM, as well as increasing its capabilities. The fine mesh requirement in dielectric rods and conducting insets is mitigated in [2] by the introduction of macro-elements in the stiffness matrix. The inclusion of lumped elements in the finite-element (FE) analysis is also appealing [3]. When the FEM is used to solve open-region scattering and radiation problems, the infinite analysis domain must be truncated to restrict the computational domain. An artificial boundary results and a boundary condition is needed. Different fashions have been proposed to handle this boundary condition. The so-called unimoment method exploits the eigenfunction expansion of the field on the artificial boundary [4], [5]. Boundary integral equations also stand for suitable boundary conditions [6], [7]. A boundary condition preserving the sparse and banded nature of the matrices arisen in the FEM is the absorbing boundary condition [8]–[10] because local boundary conditions relating the fields on the artificial boundary are considered. In addition, interest in the domain decomposition method (DDM) is becoming popular not only for enabling the use of parallel architectures, and thus reducing the CPU time compared with the traditional approach [11], but also for the new possibilities that arise. The general idea is to split the analysis domain into smaller subdomains and solve a sequence of similar subproblems on these new subdomains. In [12], the boundary conditions are adjusted iteratively by ad hoc transmission conditions of Robin type between adjacent subdomains. Further emphasis on the transmission conditions is addressed in [13]. Effective preconditioners for iterative handling of the large sparse system solution come about by considering the polynomial order of the basis functions as the decomposition domain [14]. A noniterative DDM is used in [15] saving memory requirements and computing time in the determination of the Doppler spectrum of a flying target. Likewise, a nonconforming DDM framework is also appealing [16]. There are increasing efforts in extending the FEM capabilities to analyze large problems. The case of large repeating geometries is of special interest in photonic and electromagnetic-bandgap structures. Iterative procedures exploiting geometric repetition in the DDM have been addressed in [17] and [18].

In this paper, we propose a domain decomposition scheme for design purposes. When developing a design by means of an optimization technique, the analysis domain is typically modified, e.g., its shape, the electromagnetic properties of the materials, or their shapes, until the required specifications are satisfied. It seems clear that the global structure ought to be analyzed each time a modification is carried out. However, there is no point in having to solve the whole electromagnetic problem while only a small portion of domain has changed. What we propose is to isolate those parts from the remaining analysis domain in such a way that every modification carried out on these be transparent to the remaining analysis domain, which should only be analyzed once, and thus concentrate on the analysis of those parts that evolve. In other words, we aim to use our computing

Manuscript received January 3, 2007; revised April 2, 2007. This work was supported by the Ministerio de Educación y Ciencia (MEC), Spain, under a scholarship and by the MEC under Contract TEC2004-00950/TCM.

The authors are with the Departamento de Electromagnetismo y Teoría de Circuitos, Universidad Politécnica de Madrid, 28040 Madrid, Spain (e-mail: valentin.delarubia@upm.es; jzapata@etc.upm.es).

Color versions of one or more of the figures in this paper are available online at http://ieeexplore.ieee.org.

Digital Object Identifier 10.1109/TMTT.2007.900307

resources during the optimization process only in those parts of the analysis domain that change. In order to carry out this strategy, a direct decomposition approach in the FEM is considered, and thus, the (arbitrary) subdomains are electromagnetically described by full-wave matrix-valued transfer functions, namely, admittance-type matrices. Once these transfer functions are determined, the response of the overall system is recovered by the appropriate admittance matrix connection. This methodology is compatible with a reduced-order model approach, therefore, a fast frequency sweep (FFS) technique can be carried out in the admittance-type matrices.

The general idea of splitting a domain into subdomains is rather old since it has been extensively used in different ways in the past. Our approach draws upon the mathematical literature on DDMs, and mainly upon substructuring methods with regard to the solution of partial differential equations [19]–[21]. However, further exploitation of the matrix-valued transfer function describing the electromagnetics in an arbitrary subdomain is addressed in this study.

The theory presented here relies on the formulation adopted in [22]. However, they both work on different purposes. Namely, in this paper, modifications of a given structure are actually addressed by means of a domain decomposition approach, whereas [22] deals with the incorporation of artificial ports inside a single domain, and their use in obtaining the electromagnetics within modifications of strips and slots in a given structure via a single multipurpose admittance matrix.

This paper is organized as follows. In Section II, we briefly review the FEM formulation of the boundary value problem, establish the foundations of the domain decomposition procedure, consider a model order reduction, and present the matrix connection scheme in order to restore the response of the original system. Section III deals with numerical examples and is conceived to illustrate the capabilities of the proposed approach, as well as its accuracy. Finally, in Section IV, we comment on the conclusions.

II. Formulation

Applying Galerkin projection onto an admissible function space $\mathcal{H}$, the following weak formulation is considered for the boundary value problem arisen in the time–harmonic Maxwell equations:

$$\text{Find } \bar{H} \in \mathcal{H} \text{ such that}$$
$$\int_{\Omega} \left(\frac{1}{\varepsilon_r} \nabla \times \bar{H} \cdot \nabla \times \bar{W} - k^2 \mu_r \bar{H} \cdot \bar{W} \right) dv = -\frac{jk}{\eta_0} \int_{\partial\Omega} \bar{\Psi} \cdot \bar{W} ds \qquad \forall \bar{W} \in \mathcal{H} \tag{1}$$

where ε_r and μ_r are the relative permittivity and permeability of the medium, respectively, $k = \omega\sqrt{\mu_0 \varepsilon_0}$ is the wavenumber, and $\eta_0 = \sqrt{\mu_0/\varepsilon_0}$. $\Omega \subset \mathbb{R}^3$ is a source-free bounded domain. $\bar{\Psi} = \overline{n_\Omega} \times \bar{E}$ on the boundary $\partial\Omega$ of Ω is the boundary condition, related to the tangential electric field on $\partial\Omega$, where $\overline{n_\Omega}$ is the unit outward normal vector on the boundary $\partial\Omega$, and $\bar{E}$ and $\bar{H}$ are the electric and magnetic fields [23].

The FEM is chosen to solve problem (1). In this sense, the solution to this problem requires an approximation of the solution space to be defined. Given a tetrahedral mesh of the domain Ω, the following vector functions are defined in the reference tetrahedron:

$$\text{Edge functions} \quad \begin{cases} \zeta_i \nabla \zeta_j - \zeta_j \nabla \zeta_i \\ \nabla(\zeta_i \zeta_j) \end{cases}$$
$$\text{Face functions} \quad \begin{cases} \zeta_j \zeta_k \nabla \zeta_i + \zeta_k \zeta_i \nabla \zeta_j - 2\zeta_i \zeta_j \nabla \zeta_k \\ \zeta_k \zeta_i \nabla \zeta_j + \zeta_i \zeta_j \nabla \zeta_k - 2\zeta_j \zeta_k \nabla \zeta_i \end{cases} \tag{2}$$

with $\{i, j, k\} \in \{1, 2, 3, 4\}$ and $\zeta_1, \zeta_2, \zeta_3$, and ζ_4 being the normalized coordinates for this simplex [24]. As a result, the FE space is made up of vector functions with a continuous tangential component across inter-element faces, the gradient and rotational fields have order 1 and 2, respectively. Thus far, the following linear algebraic system appears [25]:

$$(\mathbf{K}^{\Omega} - k^2 \mathbf{M}^{\Omega}) \mathbf{h}^{\mathbf{\Omega}} = -\frac{jk}{\eta_0} \mathbf{B}\mathbf{v}. \tag{3}$$

where $\mathbf{h}^{\Omega}$ is the coefficient vector of the magnetic field in Ω, $\mathbf{Bv}$ is a sparse vector, which takes into account the boundary condition, and $\mathbf{K}^{\Omega}$ and $\mathbf{M}^{\Omega}$ are sparse symmetric FE matrices, where the superscript denotes the analysis domain.

Whenever $\partial\Omega$ contains a subset Γ in which a modal spectrum can be determined, the field $\bar{\Psi}$ may be written as a linear combination of modal fields. As a result of the inclusion of the modal boundary condition in the discretization of problem (1), a matrix relationship between the tangential electric and magnetic fields on the modal boundary Γ, namely, a generalized admittance matrix (GAM), arises (see [25] for all the details). Thus,

$$\mathbf{Y} = -\frac{jk}{\eta_0} \mathbf{B}^T (\mathbf{K}^{\Omega} - k^2 \mathbf{M}^{\Omega})^{-1} \mathbf{B} \quad \mathbf{i} = \mathbf{Y}\mathbf{v}. \tag{4}$$

$\mathbf{v}$ and $\mathbf{i}$ are coefficient vectors of the modal tangential electric and magnetic field on Γ.

A. Direct Decomposition

Typically, when developing a design, only a small part of domain Ω, with reference to shape or electromagnetic properties of the media therein, is modified. However, in view of (3), the overall system ought to be solved each time a modification is carried out, which ends up in a rather time-consuming procedure that is prohibitive in most situations. What we propose is to minimize the impact of parameter modification on the overall numerical computation. In this regard, one may be interested in decomposing the analysis domain into subdomains in which the modal segmentation technique [25] cannot be applied. Thus, let $S \subset \Omega$ be the part of Ω, which should be modified. Had we known the tangential electric field on the boundary ∂S of S, the subdomain S could have been removed from the computation in Ω, decomposing problem (1) into two separate problems, concerning domains $\Omega - S$ and S. However this is not our case and, instead, our approach defines a suitable basis for the tangential electric field on the boundary ∂S, $\{\overline{\psi_i} : i = 1, \ldots, m\}$. Hence, the tangential electric field on ∂S may be expressed as

$$\overline{n_S} \times \bar{E} = \sum_i V_i (\overline{n_S} \times \overline{\psi_i}) \text{ on } \partial S \tag{5}$$

with V_i representing the coefficient of the basis function $\overline{\psi_i}$. An admissible function space for the tangential electric field is demanded. Taking advantage of the FEM context, we use piecewise (PCW) functions. Given a triangular mesh of ∂S, which indeed will be the restriction on ∂S of the tetrahedral mesh of domain Ω, the following vector functions are considered in the reference triangle:

$$\begin{matrix}\zeta_i\nabla\zeta_j - \zeta_j\nabla\zeta_i \\ \nabla(\zeta_i\zeta_j)\end{matrix} \tag{6}$$

where $\{i,j\} \in \{1,2,3\}$ and ζ_1, ζ_2, and ζ_3 are the normalized coordinates for this simplex [22]. It should be stated that tangential continuity across inter-element edges, along with completeness to order 1, are common features in this function space. The electric field in the domain Ω, related to the curl of the magnetic field in Ω, has order 1 as a result of the use of the basis functions (2) in the reference tetrahedron. This is the rational for the function space (6), where the face functions, which have order 2, are not considered. As a result, problem (1) may be decomposed in the following fashion. Without loss of generality, we assume S and Ω have disjoint boundaries in our explanation. On the one hand, regarding domain S,

$$(\mathbf{K}^S - k^2\mathbf{M}^S)\mathbf{h}^S = -\frac{jk}{\eta_0}\mathbf{b}\mathbf{V}. \tag{7}$$

where $\mathbf{K}^S$ and $\mathbf{M}^S$ are sparse symmetric FE matrices in domain S, $\mathbf{h}^S$ and $\mathbf{V}$ denote coefficient vectors of the magnetic field in S and the tangential electric field on ∂S, respectively, and $\mathbf{b}$ is a sparse matrix with elements

$$b_{ij} = \int_{\partial S} (\overline{n_S} \times \overline{\psi_j}) \cdot \overline{w_i} ds. \tag{8}$$

On the other hand, concerning domain $\Omega - S$, it follows that

$$\left(\mathbf{K}^{(\Omega-S)} - k^2\mathbf{M}^{(\Omega-S)}\right)\mathbf{h}^{(\Omega-S)} = -\frac{jk}{\eta_0}(-\mathbf{b} \quad \mathbf{B})\begin{pmatrix}\mathbf{V}\\ \mathbf{v}\end{pmatrix}. \tag{9}$$

where $\mathbf{K}^{(\Omega-S)}$ and $\mathbf{M}^{(\Omega-S)}$ are the FE matrices in domain $\Omega - S$, and $\mathbf{h}^{(\Omega-S)}$ represents coefficient vector of the magnetic field in $\Omega - S$.

In addition to having proposed a basis for the tangential electric field on the boundary ∂S, we may also consider a basis for the tangential magnetic field $\{\overline{\phi_i} : i = 1, \ldots, m\}$. In order to obtain a full-wave transfer function describing the electromagnetics either in S or in $\Omega - S$, namely, an admittance-type matrix, a mapping between the magnetic field either in S or in $\Omega - S$ and the tangential magnetic field on ∂S is required in (7) and (9). Let us consider the same basis as already defined in (6), i.e., $\overline{\phi_i} = \overline{\psi_i}, i = 1, \ldots, m$, then

$$\overline{n_S} \times \bar{H} = \overline{n_S} \times \sum_i I_i \overline{\psi_i} \text{ on } \partial S \tag{10}$$

with I_i being the coefficient of the PCW function $\overline{\psi_i}$ [22]. As a result, the following integral relationship arises:

$$\sum_i h_i \int_{\partial S} (\overline{n_S} \times \overline{w_i}) \cdot \overline{\psi_j} ds = \sum_i I_i \int_{\partial S} (\overline{n_S} \times \overline{\psi_i}) \cdot \overline{\psi_j} ds \tag{11}$$

which in matrix form reads

$$\mathbf{b}^T\mathbf{h}^S = \delta\mathbf{I}. \tag{12}$$

$\mathbf{I}$ stands for the coefficient vector of the tangential magnetic field on ∂S, and $\boldsymbol{\delta}$ is a sparse matrix with elements

$$\delta_{ij} = \int_{\partial S} (\overline{n_S} \times \overline{\psi_j}) \cdot \overline{\psi_i} ds. \tag{13}$$

This nonsingular matrix may be regarded as a change of basis in span$\{\overline{\psi_i} : i = 1, \ldots, m\}$, i.e., $\mathcal{I} = \boldsymbol{\delta}\mathbf{I}$. $\mathcal{I}$ denotes the coefficient vector of the tangential magnetic field on ∂S with respect to a new basis for the tangential magnetic field. Consequently, the following admittance-type matrix may be considered and describes the electromagnetics in S:

$$\mathcal{X} = -\frac{jk}{\eta_0}\mathbf{b}^T(\mathbf{K}^S - k^2\mathbf{M}^S)^{-1}\mathbf{b}. \tag{14}$$

Analogously, the following admittance-type matrix arises in domain $\Omega - S$:

$$\mathcal{Y} = -\frac{jk}{\eta_0}\begin{pmatrix}-\mathbf{b}^T\\ \mathbf{B}^T\end{pmatrix}\left(\mathbf{K}^{(\Omega-S)} - k^2\mathbf{M}^{(\Omega-S)}\right)^{-1}(-\mathbf{b} \quad \mathbf{B}). \tag{15}$$

To this extent, the original problem has been decomposed into two nonoverlapping subdomains where both admittance-type matrices $\mathcal{X}$ and $\mathcal{Y}$ denote the electromagnetic behavior therein. However, a link is required in order to restore the overall electromagnetics in Ω. Tangential field continuity across the boundary ∂S is what we are talking about. This requirement is achieved through a simple admittance matrix connection. Let us be more precise. The following matrix-valued transfer functions are what we have obtained by means of this formulation:

$$\begin{matrix}\mathcal{I} = \mathcal{X}\mathbf{V} \\ \begin{pmatrix}\mathcal{I}'\\ \mathbf{i}\end{pmatrix} = \mathcal{Y}\begin{pmatrix}\mathbf{V}'\\ \mathbf{v}\end{pmatrix} \\ \mathcal{Y} = \begin{pmatrix}\mathcal{Y}_{AA} & \mathcal{Y}_{Aa}\\ \mathcal{Y}_{Aa}^T & \mathcal{Y}_{aa}\end{pmatrix}.\end{matrix} \tag{16}$$

Tangential field continuity across the boundary ∂S is easily applied by imposing $\mathbf{V} = \mathbf{V}'$ and $\mathcal{I} = -\mathcal{I}'$. As a result, a GAM matrix appears as follows:

$$\mathbf{i} = \mathbf{Y}\mathbf{v} \quad \mathbf{Y} = \mathcal{Y}_{aa} - \mathcal{Y}_{Aa}^T(\mathcal{Y}_{AA} + \mathcal{X})^{-1}\mathcal{Y}_{Aa} \tag{17}$$

which definitely constitutes an alternative way of computing (4).

B. Numerical Aspects

All admittance-type matrices arising in the above formulation, (4), (14), and (15), are alike in form, viz.,

$$\mathbf{X} = -\frac{jk}{\eta_0}\beta^T(\mathbf{K} - k^2\mathbf{M})^{-1}\boldsymbol{\beta}. \tag{18}$$

Let N be the number of degrees of freedom involved in the FE discretization, i.e., the dimension of the stiffness matrix $\mathbf{K} - k^2\mathbf{M}$ and let m be the dimension of the admittance-type matrix $\mathbf{X}$, i.e., the total number of modes and PCW functions taken into account. In order to determine the admittance-type $m \times m$ matrix at a given frequency, the $\mathbf{LDL}^T$ factorization of the $N \times N$ sparse symmetric matrix $\mathbf{K} - k^2\mathbf{M}$ is carried out taking advantage of its skyline matrix storage. It should be noticed that $\boldsymbol{\beta}$ is an $N \times m$ sparse matrix. We have

$$\mathbf{X} = -\frac{jk}{\eta_0}(\mathbf{L}^{-1}\boldsymbol{\beta})^T\mathbf{D}^{-1}(\mathbf{L}^{-1}\boldsymbol{\beta}). \tag{19}$$

Therefore, (19) reads

$$\mathbf{X} = -\frac{jk}{\eta_0}\mathbf{W}^T\mathbf{D}^{-1}\mathbf{W} \tag{20}$$

where $\mathbf{W}$ is the solution to the sparse triangular system

$$\mathbf{LW} = \boldsymbol{\beta}. \tag{21}$$

As a result, an $N \times N$ sparse triangular system ought to be solved m times, a single mode or PCW function considered each time. Concerning efficiency, matrix $\boldsymbol{\beta}$ sparsity is advantageous. Let us be more precise. As suggested in [26], $W_{1j} = W_{2j} = \cdots = W_{ij} = 0$ in the jth column of $\mathbf{W}$ whenever $\beta_{1j} = \beta_{2j} = \ldots = \beta_{ij} = 0, \beta_{i+1j} \neq 0$ through the jth column of $\boldsymbol{\beta}$. Hence, by considering the position of the first nonzero element in each column of $\boldsymbol{\beta}$, the amount of operations is reduced. This information can be further used in the determination of $\mathbf{X}$ in (20). Thus,

$$(\mathbf{W}^T\mathbf{D}^{-1}\mathbf{W})_{ij} = \sum_{k=\max(p(i),p(j))}^{N} W_{ki}W_{kj}/D_{kk}. \tag{22}$$

Notice that this matrix is symmetric and, therefore, only $m(m-1)/2+m$ of their elements need to be explicitly calculated. It is clear from the above discussions that the number of operations is optimized.

C. Padé Approximation via the Lanczos Algorithm

As previously stated, all matrix-valued transfer functions arising in the proposed method have the same form. Furthermore, if we made their frequency dependence explicit, we would realize that they behave in a similar way as follows:

$$\mathbf{X}(k) = -\frac{jk}{\eta_0}\boldsymbol{\beta}^T(k)(\mathbf{K} - k^2\mathbf{M})^{-1}\beta(k). \tag{23}$$

An analytical frequency variation appears in matrix $\boldsymbol{\beta}$ whenever plane and spherical homogeneous waveguide modes and PCW functions are considered. In this sense, it should be noticed that PCW functions can properly handle inhomogeneous ports for fast frequency sweeping. Thus,

$$\boldsymbol{\beta}(k) = \boldsymbol{\beta}(k_0)\mathbf{J}_{k_0}(k) \tag{24}$$

with k_0 being a specific wavenumber and $\mathbf{J}_{k_0}$ representing a diagonal matrix with elements

$$(\mathbf{J}_{k_0}(k))_{ii} = \begin{cases} 1, & \text{for PCW functions, TEM, and spherical modes} \\ f_{k_0}(k), & \text{for TE modes} \\ 1/f_{k_0}(k), & \text{for TM modes} \end{cases} \tag{25}$$

where

$$f_{k_0}(k) = \sqrt[4]{\frac{\left(\frac{k_{c_i}}{k_0}\right)^2 - 1}{\left(\frac{k_{c_i}}{k}\right)^2 - 1}}$$

with k_{c_i} being the cutoff wavenumber of mode i. Equation (23) then reads

$$\mathbf{X}(k) = -\frac{jk}{\eta_0}\mathbf{J}_{k_0}^T(k)\mathbf{H}_{k_0}(k)\mathbf{J}_{k_0}(k) \tag{26}$$

with

$$\mathbf{H}_{k_0}(k) = \boldsymbol{\beta}^T(k_0)(\mathbf{K} - k^2\mathbf{M})^{-1}\boldsymbol{\beta}(k_0). \tag{27}$$

This symmetric matrix-valued transfer function $\mathbf{H}_{k_0}$ is symmetric matrix Padé via Lanczos (SyMPVL) compatible [27]. By choosing a wavenumber expansion point k_s and carrying out the $\mathbf{LDL}^T$ factorization of matrix $\mathbf{K} - k^2\mathbf{M}$ at this wavenumber, instead of (27), we have

$$\mathbf{H}(s) = (\mathbf{DR})^T(Id - s\mathbf{A})^{-1}\mathbf{R} \tag{28}$$

with

$$\begin{aligned} \mathbf{A} &= \mathbf{D}^{-1}\mathbf{L}^{-1}\mathbf{M}\mathbf{L}^{-T} \\ \mathbf{R} &= \mathbf{D}^{-1}\mathbf{L}^{-1}\boldsymbol{\beta}(k_0) \\ s &= k^2 - k_s^2 \end{aligned} \tag{29}$$

where $\mathbf{A}$ and $\mathbf{R}$ are square and rectangular matrices, respectively [28].

The SyMPVL algorithm generates a sequence of vectors, known as Lanczos vectors, which span the nth block Krylov subspace $\mathcal{K}_n(\mathbf{A}, \mathbf{R})$. By means of these, an nth matrix Padé approximant to (28) arises (cf. [29]) as follows:

$$\mathbf{H}_n(s) = \boldsymbol{\rho}_n^T\boldsymbol{\Delta}_n(Id - s\mathbf{T}_n)^{-1}\boldsymbol{\rho}_n. \tag{30}$$

As a result, a reduced-order model, which makes an FFS possible, is allowed.

D. Computational Aspects

The proposed approach permits the computational cost in a design procedure to be twofold: one static part, as regards $\Omega - S$, which is carried out once and might be time consuming, and a dynamic part, concerning S, which ought to be carried out each time a modification in the design parameter is carried out, and

whose computational impact needs to be minimized. This is a good strategy since numerous changes in the design parameter are normally required. Nevertheless, if we feel that the computational cost of either the static or dynamic part is not low enough, we may proceed with a further direct decomposition on that subdomain, expecting to reduce its computational impact on the overall performance. This situation is of special interest in the dynamic part since it also makes it possible to consider further changes in the objects therein such as shape modification or dielectric texturization. Section III will deal with this in greater depth. In addition, we would like to mention that this strategy allows the numerical simulation of large structures even though their numerical discretization cannot be treated as a whole on a single PC.

When a reduced-order model is used for fast frequency sweeping, special care should be taken on the frequency band where the Padé approximant converges on the original response with respect to this formulation because it is through admittance-type matrix reduced-order model connections that the response of the overall system will come about. Therefore, we are not content with some predefined order of the Padé approximation, but we require a specific convergence frequency band. This ensures all admittance-type matrix connections are accurate enough in that frequency band. In this regard, we use the technique proposed in [30], where a measurement of the error between the original response and its reduced-order model is carried out, as well as analyzing the convergence throughout different Padé approximant orders [22].

III. Numerical Results

Here, we illustrate the proposed methodology through three different devices in which we wish to carry out several modifications: a dual-mode circular waveguide filter, a hemispherical dielectric resonator antenna, and a cylindrical dielectric resonator filter. The possibilities of this approach will become apparent throughout these examples. All calculations were carried out on a laptop computer with a 1.66-GHz Intel T2300 processor and 1-GB RAM.

A. Dual-Mode Circular Waveguide Filter

In this example, we consider a four-pole elliptic dual-mode circular cavity filter. Fig. 1 shows the filter configuration, as well as its dimensions. Each circular cavity is connected to corresponding input and output WR75 rectangular waveguides by identical slots. In addition, both cavities are connected by a cross-shaped iris. Finally, each cavity is provided with a horizontal tuning screw and a $\pi/4$ tilt coupling screw.

This filter was designed in [31] by means of a hybrid mode-matching (MM) 2-D FE method to provide a 100-MHz bandwidth centred at 11.8 GHz. Here, we first analyze this structure by means of the segmentation procedure proposed in [28], where the overall domain analysis is divided into subdomains according to availability of modal field description and, therefore, analytical subdomains, or mandatory FEM resolution. This procedure circumvents the cumbersome relative convergence problem appearing in MM methods. Afterwards, we study the influence of both iris arm lengths of the cross-shaped iris on the overall filtering performance by means of the current methodology.

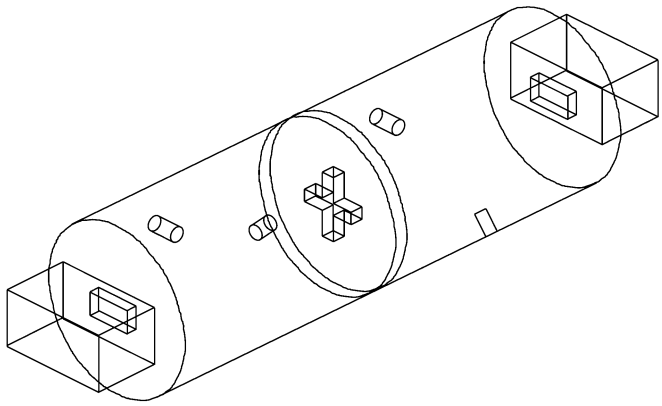

Fig. 1. Geometry of the dual-mode circular waveguide filter. Cavity length: 43.87 mm, radius: 14 mm, iris thicknesses: 1.5 mm, slot lengths: 10.05 mm, slot widths: 3 mm, arm widths: 2 mm, horizontal arm length: 7.65 mm, vertical arm length: 8.75 mm.

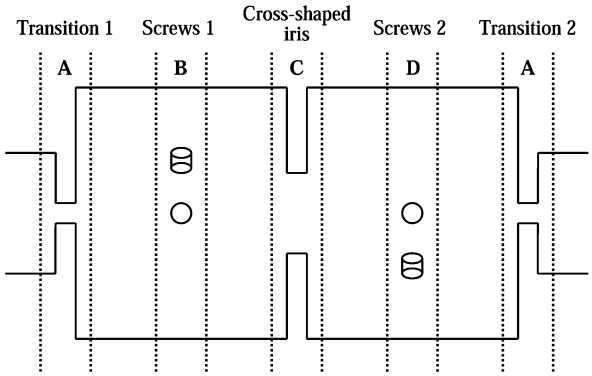

Fig. 2. Side view of the dual-mode circular waveguide filter. Modal segmentation for the analysis of the structure by means of the methodology proposed in [28].

Fig. 2 details the modal segmentation carried out in the analysis of the filter. The whole structure is assembled by joining the subdomains highlighted in Fig. 2, which are analyzed by means of the FEM, and corresponding circular waveguide sections. Since both input and output rectangular waveguide transitions to circular waveguide (transitions 1 and 2 in Fig. 2) are identical, it is only necessary to analyze one of these. Since the numerical simulation is different from that carried out in [31], it should be noticed that the tuning and coupling screw depths D_T and D_C has to be readjusted to 3.66 and 3.35 mm, respectively, in order to obtain the four-order elliptic filter response. Fig. 3 compares the results of this approach with those measured in [31]. Good agreement is achieved.

Now, we concentrate on how the filter response is affected by the cross-shaped iris when both horizontal and vertical iris arm lengths L_H, L_V are changed. Thus, we just take into account the transition between circular waveguides including the coupling iris in Fig. 2. The domain being analyzed is also shown in Fig. 4, where the subdomain splitting Ω_1, Ω_2, and S is detailed. However, subdomain S is further split, as Fig. 4(b) shows, since we want to analyze different arm lengths. As a result, the original domain is decomposed into three nonoverlapping

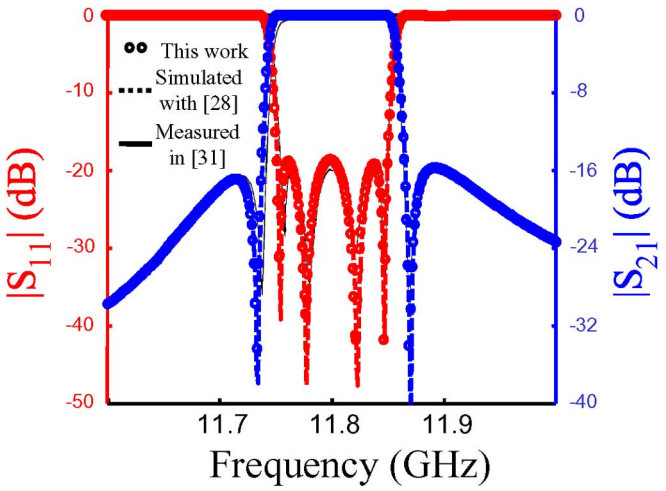

Fig. 3. Dual-mode circular waveguide filter simulation results are compared with measurements.

subdomains, i.e., Ω_1, Ω_2, and S, which, in turn, is further decomposed into 13 subdomains, the numbering of these being detailed in Fig. 4(b). Each subdomain is characterized electromagnetically by its admittance-type matrix, and straightforward admittance matrix connection reinstates the GAM of the overall circuit. It should be noted that whenever an admittance-type matrix of a cross-shaped iris decomposition subdomain is not taken into account in the matrix connection process, the subsequent GAM describes the original structure with a perfect electric conductor replacing that subdomain. Therefore, we use this procedure to determine the response of the circuit for different iris arm lengths.

Table I presents the computational cost of the static part in this approach, which concerns the determination of the admittance-type matrices for each subdomain in frequency pointwise analysis and FFS technique, constrained to converging in the band from 11.6 to 12 GHz, as well as the number of PCW functions used. On the other hand, the dynamic part in this example, the admittance matrix connection, takes no longer than 4.8 s/frequency point in all the cross-shaped iris configurations taken into account. It should be mentioned that up to 2^{13} different coupling iris configurations can straightforwardly be analyzed by means of this decomposition.

As a consequence of the discrete arm length values analyzed, this last approach just gives an idea about the role played by the cross-shaped iris in the filtering structure. Nevertheless, this strategy may be suitable, e.g., for training purposes in an artificial neural-network-based approximator scheme, where a continuous geometry variation comes about with ease. In order to carry out a full-wave continuous variation of the geometric parameter space, namely, the cross-shaped iris arm lengths, a different decomposition strategy needs to be considered. Fig. 5 proposes a continuous geometric variation compatible domain decomposition, where the whole cross-shaped iris is enclosed by the same subdomain. Thus, the original domain (region C in Fig. 2) is decomposed this time into three nonoverlapping subdomains ϖ_1, ϖ_2, and Σ. It should be noticed that, on this occasion, the whole subdomain Σ ought to be analyzed whenever a

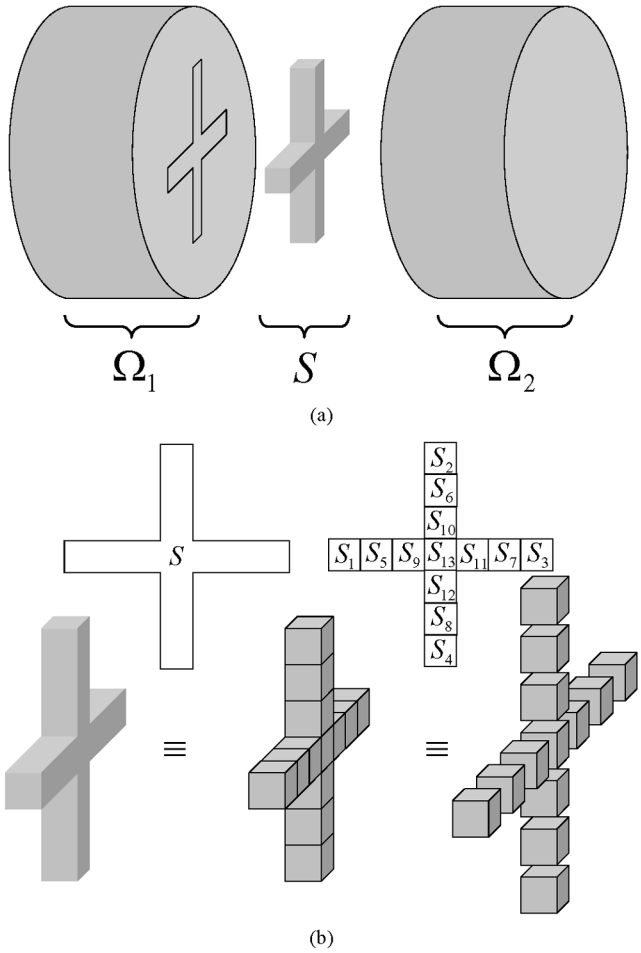

Fig. 4. Cross-shaped iris. Note that the analysis domain is the dielectric part only since perfect electric conductors are considered. (a) Decomposition of the analysis domain into subdomains. (b) Domain decomposition of the cross-shaped iris in order to allow several iris configurations.

TABLE I
STATIC PART COMPUTATIONAL RESULTS IN THE DIRECT DECOMPOSITION OF THE CROSS-SHAPED IRIS IN FIG. 4

Subdomain	PCW functions	Admittance-type matrix CPU time (s)	
		Pointwise analysis	FFS
Ω_1	416	53	155
Ω_2	416	55	225
S_1	96	0.45	1.01
S_2	96	0.36	0.76
S_3	96	0.48	0.99
S_4	96	0.34	0.77
S_5	128	0.56	1.52
S_6	128	0.50	1.38
S_7	128	0.52	1.42
S_8	128	0.45	1.53
S_9	128	0.58	1.17
S_{10}	128	0.53	1.39
S_{11}	128	0.52	1.39
S_{12}	128	0.47	1.68
S_{13}	192	0.66	3.11

modification in the cross-shaped iris dimensions is carried out. Table II details the computational cost of the static part within

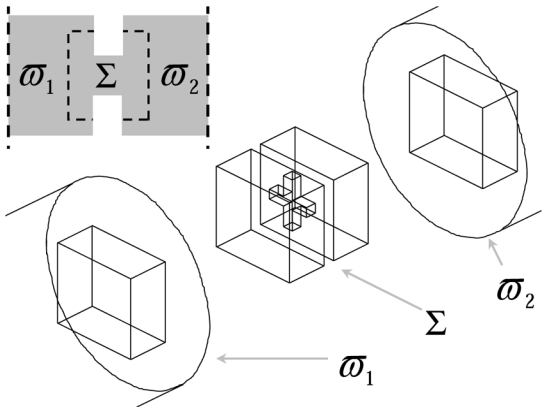

Fig. 5. Domain decomposition of the cross-shaped iris in order to allow a continuous geometric variation on the iris dimensions.

TABLE II
STATIC PART COMPUTATIONAL RESULTS IN THE DIRECT DECOMPOSITION OF THE CROSS-SHAPED IRIS IN FIG. 5

Subdomain	PCW functions	Admittance-type matrix CPU time (s)	
		Pointwise analysis	FFS
ϖ_1	130	48	147
ϖ_2	130	48	147

TABLE III
DYNAMIC PART COMPUTATIONAL RESULTS IN THE DIRECT DECOMPOSITION OF THE CROSS-SHAPED IRIS IN FIG. 5

Subdomain	PCW functions	Admittance-type matrix CPU time (s)	
		Pointwise analysis	FFS
Σ	260	23.5	124
Matrix connection CPU time per frequency point (s)			0.125

this strategy, i.e., the CPU time for the calculation of the admittance-type matrices for domains ϖ_1 and ϖ_2, constrained to converging in the band from 11.6 to 12 GHz. On the other hand, the dynamic part within this new approach is increased since whenever a modification in the iris arm lengths is carried out, not only is the admittance matrix connection process to be considered, but also the computation of the admittance-type matrix for domain Σ. Table III shows the computational cost of the dynamic part. These values are the maximum of those obtained within the different iris arm lengths analyses, constrained to converging in the band from 11.6 to 12 GHz. It should be noted that these dynamic computational costs make it possible to use the proposed methodology in a full-wave CAD-oriented strategy. The comparison of the current approach with measurements is shown in Fig. 3. Reasonable agreement is found. Fig. 6 details the filter response for different iris configurations. It can be seen how the four reflection zeros appear.

Finally, we mention that each cross-shaped iris analysis carried out with the modal segmentation procedure [28] takes 225 s/frequency point and 305 s with the FFS technique, constrained to converging in the band from 11.6 to 12 GHz. Thus, a substantial saving in computational incremental effort is accomplished by the current formulation. It should be noted that even though this filter can be analyzed by means of 2-D techniques, the proposed methodology permits the analysis of more complex structures.

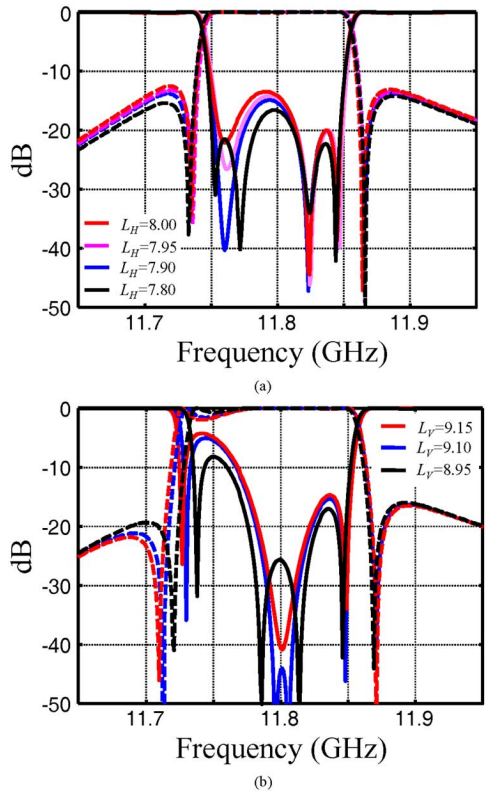

Fig. 6. Dual-mode filter responses for different iris configurations. All dimensions are in millimeters. (a) $L_V = 8.75$ mm. (b) $L_H = 7.65$ mm.

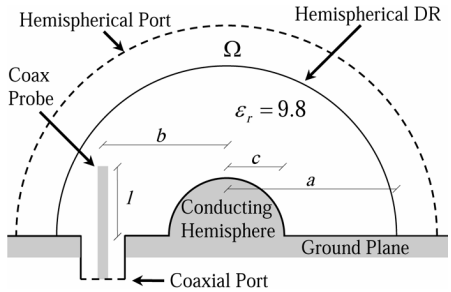

Fig. 7. Geometry of the hemispherical dielectric resonator antenna with a concentric conductor and FEM analysis domain.

B. Hemispherical Dielectric Resonator Antenna

The radiating structure geometry is detailed in Fig. 7. A hemispherical dielectric resonator of radius a with a concentric conductor of radius c is excited by a coaxial probe of length l and displacement b, as Fig. 7 shows. The dielectric resonator has a relative permittivity of 9.8. The 50-Ω coaxial line has 2 and 0.63 mm as outer and inner radii, respectively. This antenna has already been addressed in [32] using the MM method and the method of moments. In order to allow the FEM to analyze this open structure, the computational domain ought to be bounded. Inasmuch as a mode expansion is available on the boundary of the analysis domain, the FEM approach accounts for open structures. Hence, a hemisphere truncates the analysis domain since this antenna is mounted on an infinite ground plane. Thus, a

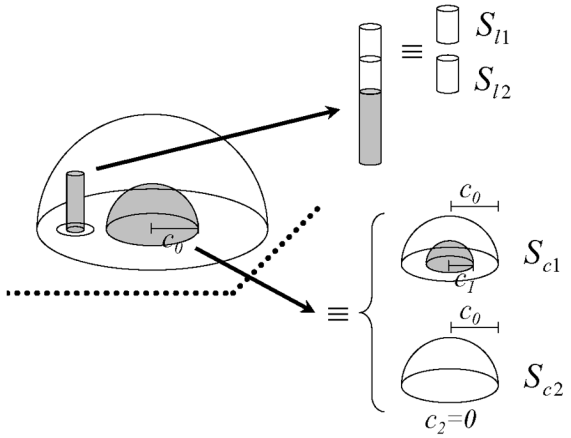

Fig. 8. Domain decomposition of the hemispherical dielectric antenna in order to modify the probe length and the concentric conductor.

hemispherical port plays the role of radiating port, meanwhile a coaxial port plays the role of exciting port. Fig. 7 also shows this. Once the computational domain Ω has been defined, we aim to study the behavior of this antenna for different concentric conductor radii and probe lengths. In this regard, we consider the cylindrical subdomains S_{l1} and S_{l2}, shown in Fig. 8, in order to enlarge or shorten the probe length l, and the hemispherical subdomain S_{c1} *or* S_{c2}, also shown in Fig. 8, conceived to account for different concentric conductor radii c_1 and c_2, respectively. Moreover, the inclusion of none of the latter subdomains in the admittance matrix connection process gives rise to a concentric conductor radius c_0, which is the decomposition hemispherical subdomain radius (see Fig. 8). It is clear that the probe length can be changed by proper consideration of subdomains S_{l1} and S_{l2} during the connection process. However, regarding concentric conductor radius modification, we could have proceeded in a similar way as before, but instead we chose to enclose the geometry to be modified under the same decomposition subdomain. Finally, we mention that the remaining analysis domain is $\Omega - S$, where $S = S_{l1} \cup S_{l2} \cup S_{c2}$.

Table IV details the number of PCW functions used and the CPU time for the determination of each admittance-type matrix in frequency pointwise computation and FFS technique. It should be noted that convergence in the band from 3.1 to 4.8 GHz is required in the FFS technique. This concerns the computational static part. In regard to the dynamic part, it takes no longer than 520 ms/frequency point to connect the admittance-type matrices. In other words, once all admittance-type matrices are determined, each full-wave analysis takes no longer than 520 ms/frequency point, which is the cost paid for the matrix connection. The results of this approach are compared with those obtained by Leung in [32] in Figs. 9 and 10. Good agreement is found. Coaxial aperture of the feeding line is considered as phase reference plane for the input impedance. We see that the antenna increases its resonance frequency as c increases, but its reactance increases as well. Furthermore, increasing l when c is fixed, increases the input impedance, while a small decrease in the resonant frequency appears, as shown in Fig. 10. Although not displayed, the responses for all combinations between c and l are possible.

TABLE IV
COMPUTATIONAL RESULTS IN THE DIRECT DECOMPOSITION OF THE HEMISPHERICAL DIELECTRIC RESONATOR ANTENNA

Subdomain	PCW functions	Admittance-type matrix CPU time (s)	
		Pointwise analysis	FFS
S_{l1}	138	1.22	4.45
S_{l2}	160	1.19	5.39
S_{c1}	210	7.64	154
S_{c2}	210	5.44	85
$\Omega - S$	440	132	547

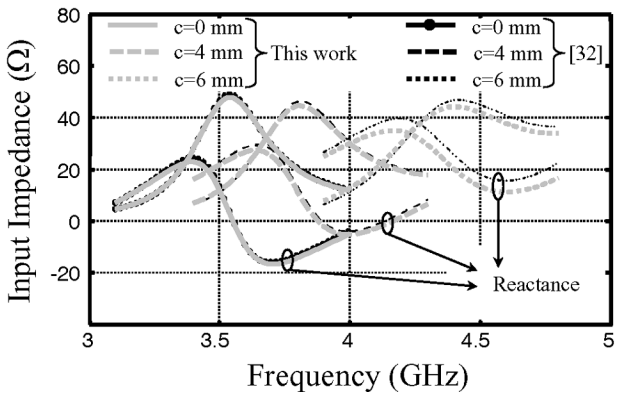

Fig. 9. Influence of the concentric conductor radius c on the input impedance in the hemispherical dielectric resonator antenna. $a = 12.5$ mm, $b = 8$ mm, $l = 7.5$ mm.

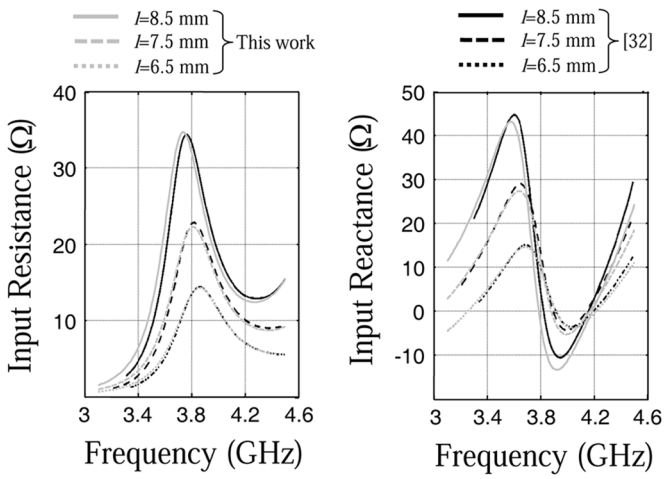

Fig. 10. Influence of the probe length l on the input impedance in the hemispherical dielectric resonator antenna. $a = 12.5$ mm, $b = 8$ mm, $c = 4$ mm.

C. Cylindrical Dielectric Resonator Filter

In this final example, we consider a coaxial-fed dielectric resonator filter made up of two cylindrical dielectric resonators with a concentric cylindrical hole of diameters d_{d1} and d_{d2}, respectively. Fig. 11 shows the geometry of this filter and details its dimensions and materials. A relative permittivity of 38 has been considered in both dielectric cylinders. This filter has already been addressed in [33] and was designed to perform a bandstop from 5 to 6.8 GHz. On this occasion, we concentrate on how this response is affected by changing the coupling to each resonator, i.e., coaxial probe lengths l_{p1} and l_{p2}, as well as the resonators themselves, modifying

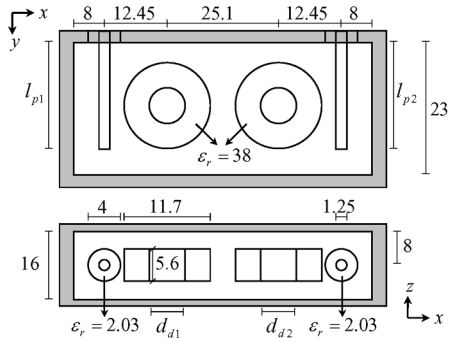

Fig. 11. Geometry of the cylindrical dielectric resonator filter. All dimensions are in millimeters.

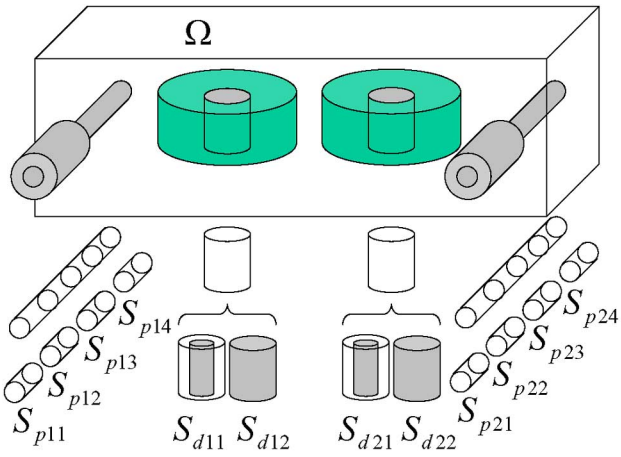

Fig. 12. Domain decomposition of the dielectric resonator filter in order to consider different probe lengths and modify the shape of the dielectric resonators.

diameters d_{d1} and d_{d2}. The direct decomposition shown in Fig. 12 is carried out in the analysis domain Ω. Concerning the coaxial probes, several cylindrical subdomains are taken into account in order to change the probe lengths, as has already been detailed in the previous example. As regards the dielectric cylinder i $(i = 1, 2)$, a concentric cylindrical subdomain is considered as a decomposition subdomain and we change the size of the dielectric resonator, i.e., diameter d_{di}, by modifying the material properties of this decomposition subdomain. Fig. 12 details all of this. Thus, subdomains $S_{p11}, S_{p12}, S_{p13}, S_{p14}, S_{p21}, S_{p22}, S_{p23}$, and S_{p24}, concerning the coaxial probes, and subdomains $S_{d11}, S_{d12}, S_{d21}$, and S_{d22}, with respect to the cylindrical resonators, come about. It should be mentioned that the remaining analysis domain $\Omega - S$, where S is the union of the former subdomains, is further split by three planes ($x = 12, x = 33$, and $x = 54$), making further use of the PCW functions, into four subdomains $\Omega_1 - S, \Omega_2 - S, \Omega_3 - S, \Omega_4 - S$, to decrease the computational cost.

Table V shows the number of PCW functions considered and the computational cost for the calculation of each admittance-type matrix in frequency pointwise analysis and FFS technique, constrained to converging in the band from 4 to 8 GHz. On the other hand, it takes no longer than 2.2 s/frequency point to connect the admittance-type matrices. This is the incremental computational effort required in order to obtain the full-wave analysis for the multiple filter configurations. It should be pointed out that this computational cost is full-wave CAD compatible. Fig. 13 shows the measurement, FEM simulation, and current formulation results for the transmission coefficient and return losses. Reasonable agreement is obtained. Finally, Fig. 14 sets

TABLE V
COMPUTATIONAL RESULTS IN THE DIRECT DECOMPOSITION OF THE CYLINDRICAL DIELECTRIC RESONATOR FILTER

Subdomain	PCW functions	Admittance-type matrix CPU time (s)	
		Pointwise analysis	FFS
S_{p11}	96	0.58	2.77
S_{p12}	112	0.67	3.44
S_{p13}	114	0.69	3.75
S_{p14}	98	0.67	2.69
S_{p21}	86	0.56	2.20
S_{p22}	112	0.66	3.47
S_{p23}	117	0.69	4.06
S_{p24}	102	0.63	2.89
S_{d11}	176	4.30	204
S_{d12}	176	4.30	105
S_{d21}	176	4.30	331
S_{d22}	176	4.30	110
$\Omega_1 - S$	330	15	201
$\Omega_2 - S$	270	18	468
$\Omega_3 - S$	292	16	393
$\Omega_4 - S$	348	17	175

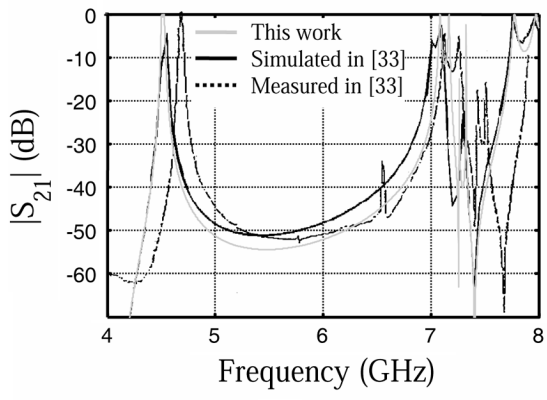

(a)

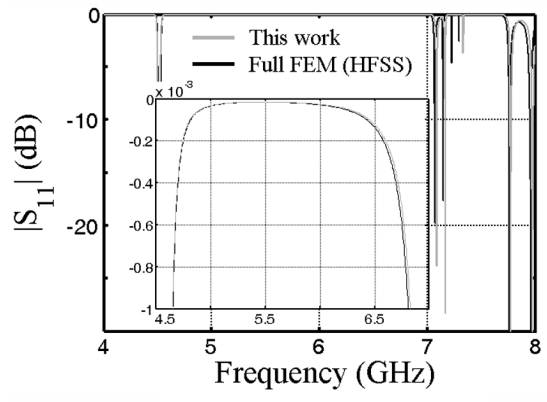

(b)

Fig. 13. Transmission and return losses of the dielectric resonator filter with $l_{p1} = l_{p2} = 20$ mm and $d_{d1} = d_{d2} = 4$ mm.

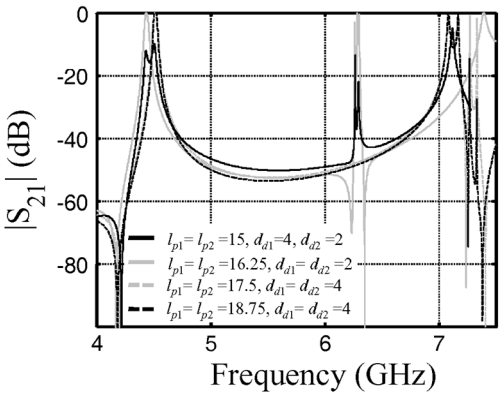

Fig. 14. Transmission in the dielectric resonator filter for different configurations. All dimensions are in millimeters.

out the transmission coefficients for different probe length and dielectric size configurations. It should be mentioned that not all configurations perform a bandstop filter from 5 to 6.8 GHz, as shown in Fig. 14.

IV. Conclusion

A direct decomposition in the FEM for design purposes has been presented. The analysis domain is explicitly divided according to the modifications that we want to consider in a given structure in order to satisfy some preestablished specifications. As a result, only those subdomains that change in the design process are analyzed, meanwhile the analysis of the remaining domain, which may be time consuming, is carried out only once. Each subdomain is electromagnetically described by a full-wave matrix-valued transfer function, an admittance-type matrix, and therefore, a suitable function basis for the boundary field description has to be proposed. Transmission conditions between subdomains are imposed through an admittance matrix connection process, ensuring a direct field continuity. An FFS procedure for the admittance-type matrices has also been considered. In addition, the matrix connection scheme is advantageous enough to allow the modification of conducting objects. Several numerical examples show the possibilities of the proposed methodology and its accuracy.

References

[1] J. M. Gil, J. Monge, J. Rubio, and J. Zapata, "A CAD-oriented method to analyze and design radiating structures based on bodies of revolution by using finite elements and generalized scattering matrix," *IEEE Trans. Antennas Propag.*, vol. 54, no. 3, pp. 899–907, Mar. 2006.

[2] Y. Zhu and A. C. Cangellaris, "Macro-elements for efficient FEM simulation of small geometric features in waveguide components," *IEEE Trans. Microw. Theory Tech.*, vol. 48, no. 12, pp. 2254–2260, Dec. 2000.

[3] M. Feliziani and F. Maradei, "Circuit-oriented FEM: Solution of circuit-field coupled problems by circuit equations," *IEEE Trans. Magn.*, vol. 38, no. 2, pp. 965–968, Mar. 2002.

[4] K. K. Mei, "Unimoment method of solving antenna and scattering problems," *IEEE Trans. Antennas Propag.*, vol. AP-22, no. 6, pp. 760–766, Nov. 1974.

[5] J. M. Jin and N. Lu, "The unimoment method applied to elliptical boundaries," *IEEE Trans. Antennas Propag.*, vol. 45, no. 3, pp. 564–566, Mar. 1997.

[6] S. P. Marin, "Computing scattering amplitudes for arbitrary cylinders under incident plane waves," *IEEE Trans. Antennas Propag.*, vol. AP-30, no. 6, pp. 1045–1049, Nov. 1982.

[7] J. M. Jin and J. L. Volakis, "A hybrid finite element method for scattering and radiation by microstrip patch antennas and arrays residing in a cavity," *IEEE Trans. Antennas Propag.*, vol. 39, no. 11, pp. 1598–1604, Nov. 1991.

[8] B. Engquist and A. Majda, "Absorbing boundary conditions for the numerical simulation of waves," *Math. Comput.*, vol. 31, no. 139, pp. 629–651, Jul. 1977.

[9] A. Bayliss, M. Gunzburger, and E. Turkel, "Boundary conditions for the numerical solution of elliptic equations in exterior regions," *SIAM J. Appl. Math.*, vol. 42, no. 2, pp. 430–451, Apr. 1982.

[10] J. P. Webb, "Absorbind boundary conditions for the finite-element analysis of planar devices," *IEEE Trans. Microw. Theory Tech.*, vol. 38, no. 9, pp. 1328–1332, Sep. 1990.

[11] Y. S. Choi-Grogan, K. Eswar, P. Sadayappan, and R. Lee, "Sequential and parallel implementations of the partitioning finite-element method," *IEEE Trans. Antennas Propag.*, vol. 44, no. 12, pp. 1609–1616, Dec. 1996.

[12] J.-D. Benamou and B. Després, "A domain decomposition method for the Helmholtz equation and related optimal control problems," *J. Comput. Phys.*, vol. 136, pp. 68–82, 1997.

[13] B. Stupfel, "A fast-domain decomposition method for the solution of electromagnetic scattering by large objects," *IEEE Trans. Antennas Propag.*, vol. 44, no. 10, pp. 1375–1385, Oct. 1996.

[14] J.-F. Lee and D. K. Sun, "pMUS (p-type multiplicative Schwarz) method with vector finite elements for modeling three-dimensional waveguide discontinuities," *IEEE Trans. Microw. Theory Tech.*, vol. 52, no. 3, pp. 864–870, Mar. 2004.

[15] P. Liu and Y. Q. Jin, "Numerical simulation of the Doppler spectrum of a flying target above dynamic oceanic surface by using the FEM-DDM method," *IEEE Trans. Antennas Propag.*, vol. 53, no. 2, pp. 825–832, Feb. 2005.

[16] C. Bernardi, Y. Maday, and A. T. Patera, "A new non conforming approach to domain decomposition: The mortar element method," in *Nonlinear Partial Differential Equations and Their Applications*, H. Brezis and J.-L. Lions, Eds. New York: Pitman, 1994, pp. 13–51.

[17] M. N. Vouvakis, Z. Cendes, and J.-F. Lee, "A FEM domain decomposition method for photonic and electromagnetic bandgap structures," *IEEE Trans. Antennas Propag.*, vol. 54, no. 2, pp. 721–733, Feb. 2006.

[18] Y. Li and J. M. Jin, "A vector dual-primal finite element tearing and interconnecting method for solving 3-D large-scale electromagnetic problems," *IEEE Trans. Antennas Propag.*, vol. 54, no. 10, pp. 3000–3009, Oct. 2006.

[19] B. Smith, P. Bjørstad, and W. Gropp, *Domain Decomposition, Parallel Multilevel Methods for Elliptic Partial Differential Equations*. New York: Cambridge Univ. Press, 1996.

[20] A. Quarteroni and A. Valli, *Domain Decomposition Methods for Partial Differential Equations*. New York: Oxford Univ. Press, 1999.

[21] A. Toselli and O. Widlund, *Domain Decomposition Methods—Algorithms and Theory*. Berlin, Germany: Springer-Verlag, 2005.

[22] V. de la Rubia and J. Zapata, "MAM—A multi-purpose admittance matrix for antenna design via the finite element method," *IEEE Trans. Antennas Propag.*, accepted for publication.

[23] J. M. Jin, *The Finite Element Method in Electromagnetics*, 2nd ed. New York: IEEE Press, 2002.

[24] J. P. Webb, "Hierarchal vector basis functions of arbitrary order for triangular and tetrahedral finite elements," *IEEE Trans. Antennas Propag.*, vol. 47, no. 8, pp. 1244–1253, Aug. 1999.

[25] J. Rubio, J. Arroyo, and J. Zapata, "Analysis of passive microwave circuits by using a hybrid 2-D and 3-D finite-element mode-matching method," *IEEE Trans. Microw. Theory Tech.*, vol. 47, no. 9, pp. 1746–1749, Sep. 1999.

[26] I. S. Duff, A. M. Erisman, and J. K. Reid, *Direct Methods for Sparse Matrices*. New York: Oxford Univ. Press, 1990, ch. 7, pp. 140–143.

[27] P. Feldmann and R. W. Freund, "Interconnect-delay computation and signal-integrity verification using the SyMPVL algorithm," in *Proc. Eur. Circuit Soc. Circuit Theory Design Conf.*, 1997, pp. 408–413.

[28] J. Rubio, J. Arroyo, and J. Zapata, "SFELP—An efficient methodology for microwave circuit analysis," *IEEE Trans. Microw. Theory Tech.*, vol. 49, no. 3, pp. 509–516, Mar. 2001.

[29] J. I. Aliaga, D. L. Boley, R. W. Freund, and V. Hernández, "A Lanczos-type method for multiple starting vectors," *Math. Comput.*, vol. 69, pp. 1577–1601, 2000.

[30] Z. Bai and Q. Ye, "Error estimation of the Padé approximation of transfer function via the Lanczos process," *Elect. Trans. Numer. Anal.*, vol. 7, pp. 1–17, 1998.

[31] J. R. Montejo-Garai and J. Zapata, "Full- wave design and realization of multicoupled dual-mode circular waveguide filters," *IEEE Trans. Microw. Theory Tech.*, vol. 43, no. 6, pp. 1290–1297, Jun. 1995.

[32] K. W. Leung, "Complex resonance and radiation of hemispherical dielectric-resonator antenna with a concentric conductor," *IEEE Trans. Microw. Theory Tech.*, vol. 49, no. 3, pp. 524–531, Mar. 2001.
[33] J. R. Brauer and G. C. Lizalek, "Microwave filter analysis using a new 3-D finite-element modal frequency method," *IEEE Trans. Microw. Theory Tech.*, vol. 45, no. 5, pp. 810–818, May 1997.

Valentín de la Rubia was born in Ciudad Real, Spain, in 1980. He received the Ingeniero de Telecomunicación degree from the Universidad Politécnica de Madrid, Madrid, Spain, in 2003, and is currently working toward the Ph.D. degree at the Departamento de Electromagnetismo y Teoría de Circuitos, Universidad Politécnica de Madrid.

His research interests include numerical methods for microwave passive circuit and antenna design.

Juan Zapata (M'93) received the Ing. Telecomunicación and Ph.D. degrees from the Universidad Politécnica de Madrid, Madrid, Spain, in 1970 and 1974, respectively.

Since 1970, he has been with the Departamento de Electromagnetismo y Teoría de Circuitos, Universidad Politécnica de Madrid, initially as an Assistant Professor, an Associate Professor in 1975, and then a Professor in 1983. He has been engaged in research on microwave active circuits and interactions of electromagnetic fields with biological tissues. His current research interest includes CAD for microwave passive circuits and antennas and numerical methods in electromagnetism, especially the FEM.

Prof. Zapata is a member of the Editorial Board of the IEEE TRANSACTIONS ON MICROWAVE THEORY AND TECHNIQUES.